*Regenerative Biomaterials*, 2021, 1–13
doi: 10.1093/rb/rbab052
Research Article

# Fabrication and evaluation of an optimized xenogenic decellularized costal cartilage graft: preclinical studies of a novel biocompatible prosthesis for rhinoplasty

**Shuang Lin[1,2], Yuanjia He[3], Meihan Tao[2], Aijun Wang[4] and Qiang Ao [2,5,*]**

[1]Department of Plastic Surgery, Shengjing Hospital of China Medical University, 36 Sanhao Street, Shenyang 11004, China [2]Department of Tissue Engineering, China Medical University, 77 Puhe Road, Shenyang 110112, China [3]Department of Stomatology, The Fourth Affiliated Hospital of China Medical University, 4 Chongshan East Road, Shenyang 110033, China [4]Surgical Bioengineering Laboratory, Department of Surgery, School of Medicine, University of California Davis, Sacramento, CA 95817, USA [5]Institute of Regulatory Science for Medical Device, National Engineering Research Center for Biomaterials, Sichuan University, 24 Yihuan Street, Chengdu 610065, China

*Correspondence address. Department of Tissue Engineering, China Medical University, 77 Puhe Road, Shenyang 110112, China. E-mail: aoqiang@tsinghua.edu.cn

Received 27 April 2021; revised 21 August 2021; accepted on 2 September 2021

## Abstract

On account of the poor biocompatibility of synthetic prosthesis, millions of rhinoplasty recipients have been forced to choose autologous costal cartilage as grafts, which suffer from limited availability, morbidity at the donor site and prolonged operation time. Here, as a promising alternative to autologous costal cartilage, we developed a novel xenogeneic costal cartilage and explored its feasibility as a rhinoplasty graft for the first time. Adopting an improved decellularization protocol, in which the ionic detergent was substituted by trypsin, the resulting decellularized graft was confirmed to preserve more structural components and better mechanics, and eliminate cellular components effectively. The *in vitro* and *in vivo* compatibility experiments demonstrated that the decellularized graft showed excellent biocompatibility and biosecurity. Additionally, the functionality assessment of rhinoplasty was performed in a rabbit model, and the condition of grafts after implantation was comprehensively evaluated. The optimized graft exhibited better capacity to reduce the degradation rate and maintain the morphology, in comparison to the decellularized costal cartilage prepared by conventional protocol. These findings indicate that this optimized graft derived from decellularized xenogeneic costal cartilage provides a new prospective for future investigations of rhinoplasty prosthesis and has great potential for clinical application.

**Keywords:** decellularization; costal cartilage; extracellular matrix; prosthesis; rhinoplasty

## Introduction

At present, the widely used rhinoplasty prostheses include autologous grafts, mainly costal cartilage, and synthetic grafts such as silicone and expanded polytetrafluoroethylene [1]. Owing to poor biocompatibility of synthetic grafts, millions of recipients were forced to choose autologous costal cartilage as grafts [2, 3]. However, autologous cartilage grafts suffer from multiple shortcomings, including severe morbidity at donor site, extremely limited availability and prolonged operation time. In particular, there are inevitable thoracic scars and deformities, which lead to severe pain for recipients and affect their aesthetics [4, 5]. Therefore, there is a need for new biomaterials as rhinoplasty prostheses.

Decellularized cartilage grafts emerged as promising alternatives for repairing cartilage defects with special attention. The advantage of this biomaterial is that the micro-environment of native extracellular matrix (ECM) in tissue or organ is preserved which still contains a variety of appropriate bioactive elements without the presence of cellular and nuclear components, thus avoiding potential immunological rejection. It allows for a xenogenic approach to substitute autologous tissue which is attributed to ECM proteins highly conserved across species. A multitude of studies on the use of acellular cartilage to repair various cartilage defects have been reported [6, 7]. Regardless of the application in plastics or orthopedics, the physical and chemical properties of acellular cartilage determine its therapeutic effect as a scaffold structure. Many methods have been devised to prepare decellularized cartilage. The conventional method is based on multiple cycles of treatment with ionic detergents including sodium dodecyl sulfate and sodium deoxycholate [8, 9]. Although this method has been proven to achieve proper removal of cellular components, it causes severe loss of proteoglycans and cytokines, along with the significant decrease in mechanical strength.

The effects of various decellularization methods vary widely. Physical methods such as agitation, osmotic pressure shock and freezing–thawing have little effect on ECM, but decellularization efficiency is very limited especially for dense tissues [10, 11]. Detergent treatment involved in chemical methods is the most commonly used method. Ionic detergents are effective in rupturing cytoplasmic and nuclear membranes, but tend to denature proteins by disrupt protein–protein interactions [12, 13]. Non-ionic detergents are significantly better than ionic ones in protecting ECM, while they are often inadequate for decellularization when used alone [14]. As confirmed in previous studies, trypsin causes the loss of attachment activity in chondronectin, since the chondronectin plays an important role in the binding of cells with ECM [15]. In addition, trypsin is a commonly used reagent for cell experiments, which has the characteristics of low toxicity and being inactivated by serum, so it has little deleterious effect on the biosecurity of the graft [16]. Therefore, in this study, we tried to replace ionic detergent with trypsin, and compared the effects of the two protocols on decellularization efficiency, chemical and mechanical properties.

To our knowledge, only few decellularization protocols for costal cartilage have been reported, and there is no report about decellularized xenogeneic costal cartilage as a rhinoplasty graft. In the present study, the optimized decellularized grafts were fully characterized and assessed on their compositional, mechanical and biocompatible properties, as well as functional evaluation in comparison with conventional decellularized grafts.

## Materials and methods

### Fabrication of decellularized costal cartilage

Porcine costal cartilage was harvested from pigs (average age 6–8 months and weight 110–120 kg) according to the Standard NOM-062-ZOO-1999 [17]. All animal-related experiments in this study were approved and monitored by the Institutional Animal Care and Use Committee (IACUC) of China Medical University (CMU2019268).

There are 14 pairs of costal cartilages per pig, and the 6th to 8th pairs were selected owing to their suitable length, thickness and angle. After the removal of surrounding muscle and perichondrium, the costal cartilage was carved using the commercial silicone rhinoplasty prosthesis as a mold (Fig. 1A and B). Then, the materials were immersed in phosphate-buffered saline (PBS) solution at 4°C for further assessment. The carved cartilages were randomly divided into the following three groups.

***Natural costal cartilage (NCC).*** It consists of natural cartilage as a control group for all assays.

***Sodium deoxycholate-based decellularized costal cartilage (SDCC).*** This protocol slightly modified the decellularization protocol proposed by Baiguera *et al.* [18] (Fig. 1C). Following the immersion in distilled water (DW) for 2 h, the cartilage was incubated in 4% sodium deoxycholate (w/v) (Sigma, St. Louis, MO) for 4 h. After rinsing twice with DW, the tissue was treated with 1% Triton X-100 (v/v) (Sigma) for 4 h, and then incubated in 100 U/ml Deoxyribonuclease I (DNase I) solution (Sigma) for 3 h at 37°C. Finally, another two more rinses with DW were carried out. The above process was repeated 15 cycles. The above processes were performed at room temperature with constant stirring at 120 rpm, except for special instructions.

***Combination method-based decellularized costal cartilage (CDCC).*** It is further modified on the basis of ionic detergent decellularization protocol, replacing ionic detergent with trypsin and combining with the non-ionic detergent (Fig. 1C). Briefly, after the immersion in DW for 2 h, the cartilage was treated with 1% trypsin (w/v) (Sigma) for 6 h, and the enzyme solution was changed freshly every 2 h. Following another two washes in DW, the cartilage was submersed in 1% Triton X-100 solution (v/v) for 4 h. Subsequently, the cartilage was subjected to nuclease digestion with 100 U/ml DNase I solution at 37°C for 3 h. Finally, two rinses with DW were performed. The above process was repeated 15 cycles. The above processes were carried out at room temperature with constant stirring at 120 rpm, except for special instructions.

### Histological and immunohistochemical staining

Following fixation in 4% paraformaldehyde solution for 24 h, the decellularized specimens were paraffin embedded and sectioned into 5 μm slices. After being subjected to dehydration, deparaffinization, rehydration and wash with DW, the specimens were subsequently stained with the following dye solution. Hematoxylin–eosin (HE) and 4′,6-diamidino-2-phenylindole (DAPI) were performed to evaluate the removal of cellular and nuclear components.

Safranin O staining was used to detect the presence of glycosaminoglycans (GAGs), which is one of the main important components of hyaline cartilage, and affects mechanical properties and biocompatibility. Type II collagen was immunolocalized with rabbit anti-human type II collagen polyclonal antibody (1:100, Abcam, Cambridge, MA), followed by incubation with horseradish peroxidase-conjugated anti-mouse antibody (1:200, Abcam) and chromogenic reaction with diaminobenzidine tetrahydrochloride (DAB, Abcam).

### Quantitative detection for DNA and main structural components

The effectiveness of decellularization protocols was further analyzed by quantifying the remaining DNA in grafts. The TIANamp Genomic DNA Kit (Takara, China) was used to extract DNA from the samples of each group according to the manufacturer's instruction. Then, the extracted DNA was quantified with BioDrop (BioLion, UK). Besides, the remnant DNA fragments were measured by the semi-quantitative agarose gel electrophoresis test.

A hydroxyproline quantification assay with Hydroxyproline Assay Kit (Sigma) was performed to determine the total collagen content of each group according to the manufacturer's instruction.

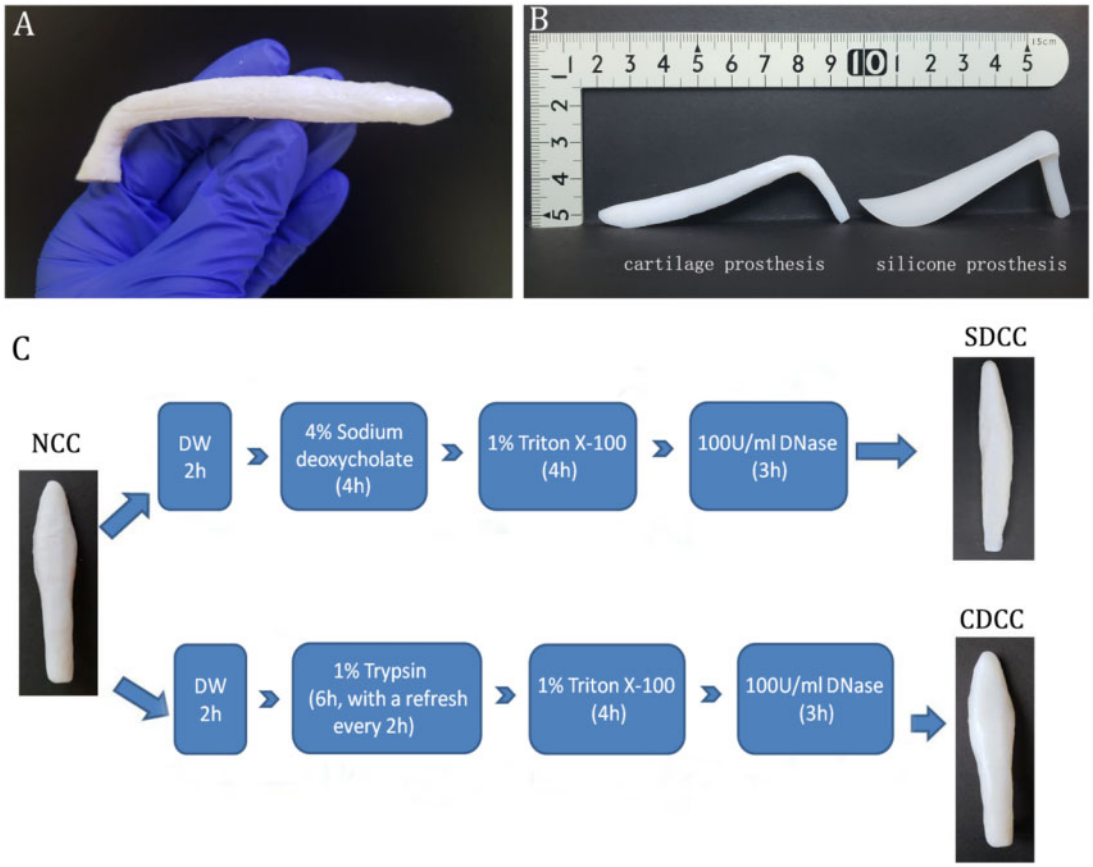


**Figure 1.** Fabrication of decellularized costal cartilage grafts. (**A**) The untreated porcine costal cartilage. (**B**) The carved cartilage using the commercial silicone rhinoplasty prosthesis as a mold. (**C**) The decellularization protocol of sodium deoxycholate-based decellularized costal cartilage (SDCC) and combination method-based decellularized costal cartilage (CDCC).

This assay takes advantage of the characteristic that hydroxyproline is mainly limited to collagen and uses it as an indicator of total collagen content. The amount of total collagen was calculated according to the ratio of hydroxyproline to collagen, which was 1:7.69.

GAGs content of grafts in three groups was assessed using Dimethylmethylene Blue Assay Kit (GenMed) following the manufacturer's instructions.

There are five replicate samples in each group in all quantitative tests, and the data are normalized to dry weight.

### Scanning electron microscopy assessment

Scanning electron microscopy (SEM) was used to observe the microstructure of samples. The samples were fixed in 0.25% glutaraldehyde (Sigma) for 2 h and rinsed with PBS for 15 min three times. After dehydration through a graded series of ethanol, samples were critical-point dried with carbon dioxide. Afterwards, the samples were sputter coated with gold and observed under VEGA3 tungsten scanning electron microscope (TESCAN, Czech).

### Mechanical analysis

An Electric Dynamic Test System (Shenyang, China) was conducted for detecting elastic and compressive properties. Prior to the test, the samples were processed into the shape suitable for the test chamber and incubated in PBS at room temperature for 2 h. Both ends of the sample were attached to a custom-made instrument to keep the starting distance between the two instruments constant at 10 mm. Parameters including the Young's modulus, stress at fracture and strain at fracture were collected and calculated. Five replicate samples per group were tested and analyzed.

## Biocompatibility evaluation

### Isolation and culture of chondrocytes and fibroblasts

The chondrocytes were harvested from the nasal septum of Sprague-Dawley rats. Briefly, the nasal septal cartilage was carefully dissected out and washed three times with PBS. After the perichondrium was removed, the cartilage was incubated with 0.25% trypsin for 30 min at 37°C. Then, the cartilage was cut into small pieces and incubated with collagenase type II (Sigma) on a rotator for 4–5 h at 37°C until the solid cartilage pieces disappeared. Subsequently, the cell pellet was washed and incubated in Dulbecco's/Ham's F-12 medium (DMEM/F12) (Gibco, USA) containing 10% fetal bovine serum (FBS) (Gibco) and 1% penicillin/streptomycin (P/S) (Gibco). The medium was refreshed every 72 h and when the confluence reached 80%, the cells were passaged at a ratio of 1:2–1:3. The second to fourth generation cells were harvested and identified by toluidine blue staining (Fig. 5A) and type II collagen immunofluorescence staining (Fig. 5B).

L929 fibroblasts were purchased from the Basic Medical Cell Center of the Institute of Basic Medicine, Chinese Academy of Medical Sciences. The cells were cultured in DMEM/F12 supplemented with FBS and P/S. The cells are cultured in an incubator (37°C, 5% $CO_2$) and passaged to harvest sufficient numbers for future assessment.

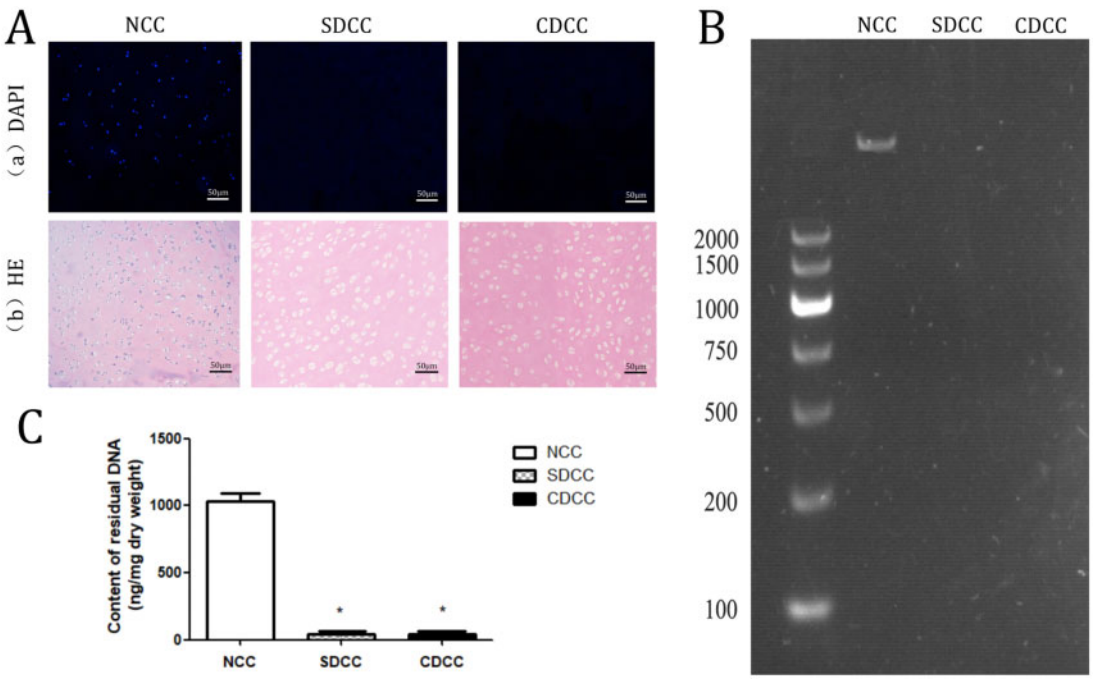


**Figure 2.** Evaluation of decellularization effect. The DAPI (**Aa**) and HE (**Ab**) were carried out to assess the elimination of cells. The residual DNA was tested by agarose gel electrophoresis (**B**) and quantification of residual DNA content (**C**). Data are expressed as the mean ±SD ($n = 5$). *$P < 0.05$ compared with NCC.

## Observation of cell affinity

The adhesion and survival of fibroblasts on the graft surface were assessed by SEM to evaluate the cell affinity of the material. The cell density of the fibroblast suspension was adjusted to $1 \times 10^4$/ml, and then co-culture with the two groups of grafts. After 3 days, the medium was aspirated, the cell-material complex was washed with PBS for three times, and then fixed with glutaraldehyde and osmium acid, dehydrated with gradient alcohol, dried, quenched and sprayed with gold, and finally observed under SEM.

## Detection of released DNA content in culture medium

DNA released from chondrocytes with ruptured cellular membranes was detected as an assessment of the extent of damaged cells. After the chondrocytes at a density of $1 \times 10^4$/ml were co-cultured with the grafts of 1 cm × 1 cm × 0.3 cm for 3 days, the culture medium was extracted and the DNA content in it was tested to analyze the biocompatibility and biosecurity of grafts. The negative and positive control groups were chondrocytes cultured without any samples and with 2% Triton X-100, respectively. Five replicate samples were set in each group, the absorbance at 260 nm was measured and the mean value was calculated.

## Cytotoxicity analysis

To evaluate the cytotoxicity of the grafts, probably generated in the process of decellularization and/or sterilization, Cell Counting Kit-8 (CCK-8) was performed following the manufacturer's instructions. Briefly, the extracted medium was harvested by incubating 100 mg samples of SDCC and CDCC in 1 ml medium at 37°C for 72 h. Besides, negative, positive and blank control groups were prepared by incubating chondrocytes with polyethylene, DMSO and without cells, respectively. The chondrocytes were plated at a density of $1 \times 10^4$ cells per well in 96-well plates, and then cultured at 37°C with 5% $CO_2$. Cell proliferation was evaluated at 24, 48 and 72 h, respectively. At each time point, 10 µl of CCK-8 solution was added to each well, followed by incubation at 37°C for another 2 h. Optical density was measured at 450 nm, and the mean value derived from five replicates for each group was calculated.

## Subcutaneous implantation experiment

Subcutaneous implantation experiment was performed to evaluate the acute inflammatory response in the short term after implantation of the graft. In addition to 20 rats in the blank group, SDCC and CDCC were randomly implanted subcutaneously into the backs of a total of 40 rats (male, 12 weeks old, weighing 200 g). Each group of grafts was cut into a size of 1 cm × 1 cm × 0.3 cm. After the general anesthesia, an incision was made on the left and right sides of the rat's back. The subcutaneous pocket was separated from the incision upward. The grafts of two groups were implanted subcutaneously on the backs of rats (Fig. 6A). The blank group only created the subcutaneous pocket without implanting the grafts.

The rats were sacrificed by $CO_2$ at 3, 7, 14 and 28 days after the operation. The blood of rat was harvested from eye veins to harvest serum for ELISA using Quantikine IL-2 Elisa Kit (R&D, USA), Quantikine IL-4 Elisa Kit (R&D) and IFN-γ Elisa Kit (NOVUS, USA), which were employed to assess the possible systemic immune response caused by acellular xenogeneic graft.

In addition, the grafts with adjacent tissues were collected and fixed in 4% paraformaldehyde. Paraffin sections were made and stained for CD 11b immunohistochemistry, which was used to observe the density and distribution of neutrophils and evaluate local immune response to SDCC and CDCC. Briefly, following antigen retrieval, endogenous peroxidases inactivation and serum blocking, the sections were treated with primary antibody against CD 11b (rabbit anti-CD 11b antibody, Abcam) at 4°C overnight. Subsequently, the secondary antibody (goat anti-rabbit IgG1, Abcam) was used for 30 min after three washes with PBS. Finally, DAB chromogenic reaction and hematoxylin counterstaining were carried out sequentially. The number of CD 11b positive cells was

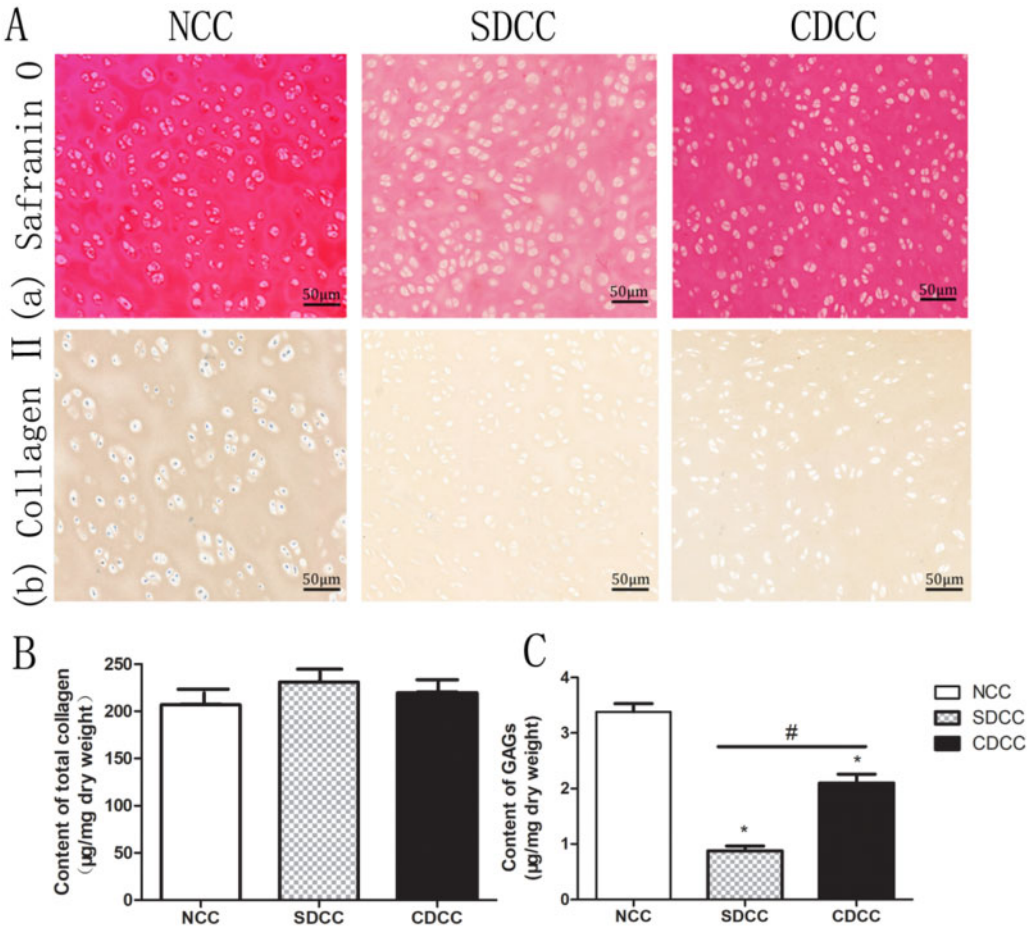


**Figure 3.** Evaluation of biochemical properties. The safranin O (**Aa**) and type II collagen immunohistochemical (**Ab**) staining revealed the distribution and alteration of the main components of cartilage before and after decellularization. The assessment of total collagen (**B**) and GAGs (**C**) demonstrated that the effect of different decellularization protocols on ECM. $^{*}P < 0.05$ compared with NCC, $^{\#}P < 0.05$ compared with SDCC.

counted at ×200 magnification with five areas per sample, and quantification was performed by Image-Pro plus software.

### *In vivo* study for functionalities

***Surgery procedure.*** Since the tissue level (from shallow to deep: epidermis, dermis, muscle, periosteum and bone) and the area size of the nasal dorsum of rabbit is similar to that of the human body, adult rabbits were used as animal models for *in vivo* functionality experiments. Twenty-four New Zealand white rabbits (male, 10–12 weeks old, weighing 3.0–4.0 kg) were fed standard food and unlimited water supply under 12 h light cycle, and randomly divided into two groups with 12 rabbits in each group, including SDCC and CDCC group. Firstly, rabbits were fasted for 12 h with free access to water. Following induction of anesthesia with intraperitoneal injection of a mixture of ketamine (50 mg/kg) and acepromazine (0.05 mg/kg), the rabbits underwent standard endotracheal general anesthesia after induction. And the general anesthesia was kept by isoflurane gas (as needed). After shaving and desinfection, a 1.5-cm long incision was made at 2 cm above the tip of the nose to reach the periosteal surface. The cavity in the lower layer of the muscle (the upper layer of the periosteum) was created, with an area of about 5 cm × 1.5 cm, and the uppermost end reached between the two eyes. Then, the graft was gently held and placed into the cavity. Afterwards, the incision was sutured intermittently with 6-0 absorbable sutures. Finally, all rabbits were injected intramuscularly with penicillin and meloxicam for 3 consecutive days to prevent infection and relieve pain.

***Imaging examination.*** Since cartilage components are well displayed in magnetic resonance imaging (MRI), MRI was performed at 3 and 6 months to evaluate the size, morphology and relationship between the graft and surrounding tissue *in vivo*. After anesthesia, the rabbit was placed in a prone position on the examination table, and a metal magnetic ring was fixed on its face. The sagittal position was selected for scanning because the graft scanned at this angle has a comprehensive imaging effect.

***Histological and biochemical analyses.*** At the 6 months after the operation, the rabbits were euthanized by overdose of 1% sodium pentobarbital. The grafts and adjacent tissues were harvested and underwent histological and biochemical analyses.

In the HE staining, the gross morphology and inflammation of samples were evaluated. The junction between the graft and the surrounding tissue was randomly selected, and a low magnification field of view (10 × 10) was used to choose an area with a large number of inflammatory cells (neutrophils, eosinophils, basophils, lymphocytes and monocytes). Then five fields in high magnification field of view (10 × 40) were selected to observe and count the number of inflammatory cells, and the average value was calculated.

In addition, Safranin O staining, GAGs quantification assay and type II collagen immunohistochemistry were performed to evaluate

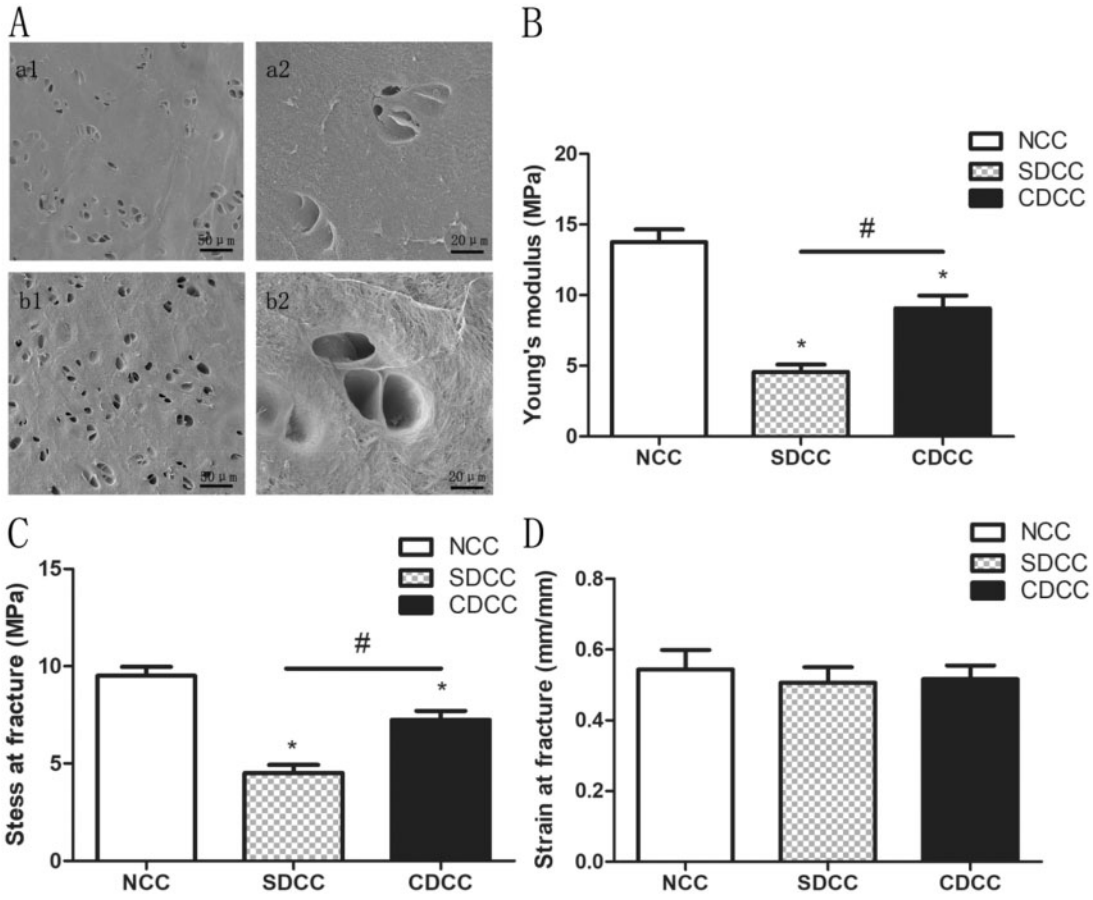


**Figure 4.** Evaluation of microstructure and mechanical properties. (**A**) The microstructure of SDCC and CDCC under SEM. **a1** and **a2** showed that chondrocytes in SDCC were removed, but the lacuna structure after decellularization was destroyed. **b1** and **b2** showed that the cells in CDCC were completely eliminated with lacuna in good shape. Young's modulus (**B**), stress at fracture (**C**), and strain at fracture (**D**) were assessed to evaluate mechanical characteristics of NCC, SDCC and CDCC. $^{*}P < 0.05$ compared to NCC, $^{\#}P < 0.05$ compared to SDCC.

the changes in main compositions of the grafts before and after the *in vivo* implantation, which were used to investigate the degradation and absorption of the grafts.

### Statistical analysis

All quantitative results were represented as mean ± standard deviation (SD) and statistical analysis was performed using GraphPad Prism 5.0 software (USA). The differences between two groups were analyzed by Student's *t*-test, and differences between multiple groups were compared by one-way analysis of variance. $P < 0.05$ was considered to be statistically significant.

## Results

### Preparation and decellularization effects of grafts

After the decellularization process, both SDCC and CDCC maintained their original length, width, thickness and morphology, but became more whitish and softer. In particular, SDCC is more transparent and loose than CDCC (Fig. 1C). The two protocols of decellularization in this study fulfilled the relevant criteria [10]. No intact cell or nuclei were visible by HE staining, and no visible nuclear component was found in DAPI staining (Fig. 2A). The residual DNA contents in SDCC and CDCC were dramatically less than that in native cartilage tissue ($P < 0.001$) and reached the criterion of 50 ng/mg (Fig. 2C). Furthermore, no visible DNA band of SDCC and CDCC was detected in agarose gel electrophoresis (Fig. 2B).

### Biochemical properties

To investigate distribution of GAGs within the grafts of three groups, samples were processed by Safranin O staining. The result exhibited that SDCC and CDCC were lightly stained compared with NCC (Fig. 3A). It is worth mentioning that there were obviously more GAGs retained in CDCC than in SDCC. The immunohistochemical staining of each group showed brownish yellow without obvious difference, indicating that SDCC and CDCC preserve the main matrix component of type II collagen (Fig. 3A).

Biochemical assays were employed to quantitatively assess the contents of main structural components including total collagen and GAGs. Concerning total collagen content, CDCC and SDCC showed a slight increase compared with NCC, but there was no significant difference ($P > 0.05$) (Fig. 3B). In terms of GAGs, the quantitative assay suggested that SDCC and CDCC were significantly lower than NCC, while the GAG content of CDCC was significantly higher than that of SDCC ($P < 0.05$) (Fig. 3C).

### Microstructure

The characterization of microstructure in NCC, SDCC and CDCC was determined by SEM. The ultrastructure of CDCC has no

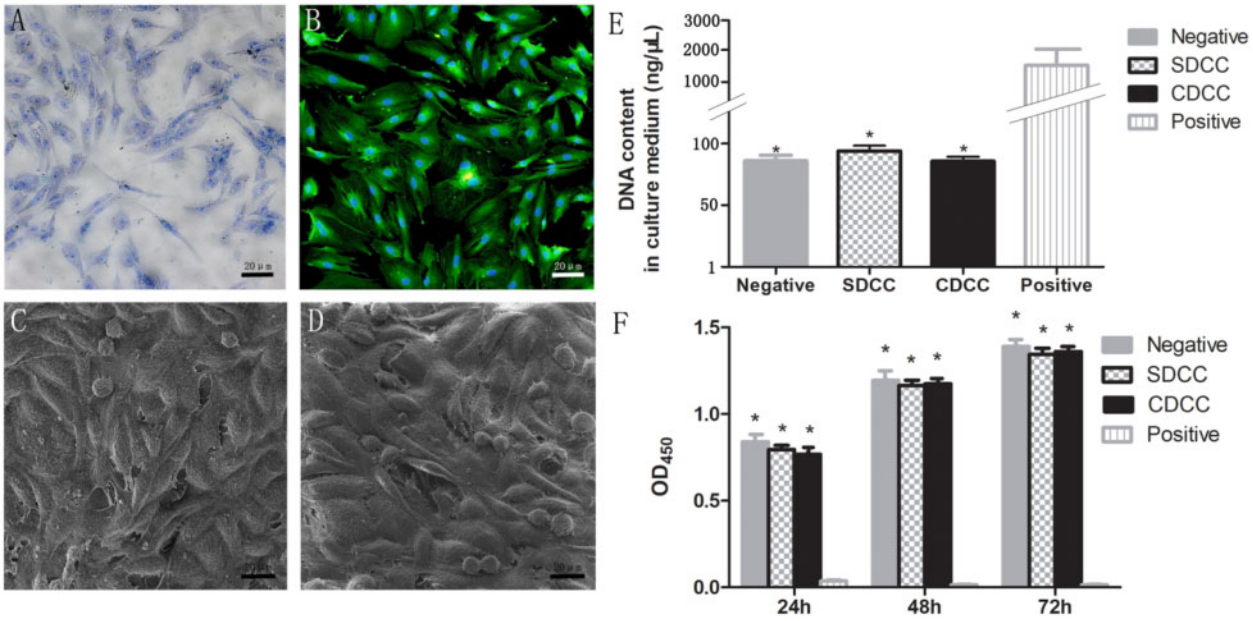


**Figure 5.** *In vitro* biocompatibility assay. (**A**) Toluidine blue staining of nasal septal chondrocytes. (**B**) Type II collagen immunofluorescence staining of chondrocytes. (**C**) Fibroblasts could survive and proliferate on the surface of CDCC. (**D**) The fibroblasts could be seen to survive and proliferate on SDCC. The assay of released DNA in the medium (**E**) and CCK-8 test of extract medium (**F**) were conducted to assess the cytocompatibility and cytotoxicity of CDCC and SDCC. $^{*}P < 0.05$ compared with positive control.

obvious changes after decellularization, preserving its intact collagen fiber and lacuna morphology (Fig. 4A, a1, a2). The collagen fibers of SDCC remained basically unchanged, but the morphology of the chondrocyte lacunae changed significantly, becoming shallower or ruptured (Fig. 4a, b1, b2).

## Mechanical properties

For the rhinoplasty, the grafts need to exhibit mechanical strength and stability after the *in vivo* implantation, enabling load bearing and stress transferring, and maintaining the original morphology of the grafts, which is vital for *in vivo* experiments and further clinical application. The obtained parameters revealed that the Young's modulus (elastic property) and stress at fracture (compressive property) of SDCC and CDCC were both noticeably lower than NCC ($P < 0.05$), but these two parameters of CDCC were remarkably higher than those of SDCC ($P < 0.05$). Moreover, the strains at fracture of all groups were comparable ($P > 0.05$) (Fig. 4B–D).

## Evaluation of biocompatibility

***Cell affinity analysis.*** The survival of cells on the surface of the materials can be observed under SEM to evaluate the cell affinity of two decellularized grafts. After fixation and dehydration, it was observed that the cells could adhere and survive, along with newly proliferating cells in a spherical shape, indicating that CDCC graft has no toxicity on fibroblasts (Fig. 5C). The fibroblasts could also adhere and survive on SDCC (Fig. 5D).

***Released DNA content in culture medium.*** The main potential risk of decellularized graft is the inability to adequately remove detergents used for decellularization, which may have an adverse effect on biosecurity and biocompatibility [19, 20]. Detergents that are not completely removed will cause a large number of host cell rupture and death after implantation, resulting in a significant increase in the DNA content in the culture medium. There was no significant difference in the DNA content in the culture medium between the two decellularized groups ($P > 0.05$). Meanwhile, the results of SDCC and CDCC exhibited no significant difference compared with the negative group ($P > 0.05$), but they were remarkably lower than that of positive control ($P < 0.05$) (Fig. 5E). It was revealed that both SDCC and CDCC have excellent biosecurity and biocompatibility.

***Cytotoxicity.*** As a supplement to provide a comprehensive analysis of biocompatibility, CCK-8 assay was performed to determine the cytotoxicity of SDCC and CDCC. At 24, 48 and 72 h, respectively, the $OD_{450}$ of the two grafts were comparable, and there was no statistical difference compared with the negative control group (Fig. 5F). The data demonstrated that SDCC and CDCC had good biocompatibility and no toxicity on chondrocytes.

## Analysis of acute inflammatory response

All sixty rats survived to the scheduled time point of sampling without infection or death. The ELISA assay of serum demonstrated that, on the 3rd and 7th day after operation, the IL-2 and IFN-γ of SDCC group and CDCC group were significantly higher than those of the blank group ($P < 0.05$). On the 14th day, the SDCC group was higher than the blank group ($P < 0.05$), and there was no statistical difference between the CDCC group and the blank group ($P > 0.05$). On the 28th day, there was no significant difference in IL-2 and IFN-γ among the blank group, SDCC group and CDCC group ($P > 0.05$). On the 3rd, 7th, 14th and 28th day after operation, there was no significant statistical difference in IL-4 among these three groups ($P > 0.05$) (Fig. 6B–D).

The immunohistochemistry of CD11b (+) neutrophils is mainly used to evaluate the local immune response after foreign graft implantation. In the SDCC and CDCC groups, the number of CD11b (+) cells gradually increased between the 3rd and 7th days. On the 14th day, positive cells were presented less than before. On the 28th day, the staining of the two groups was significantly lighter than before, and there was no obvious difference between the two groups (Fig. 6F). The quantitative analysis of immunohistochemical

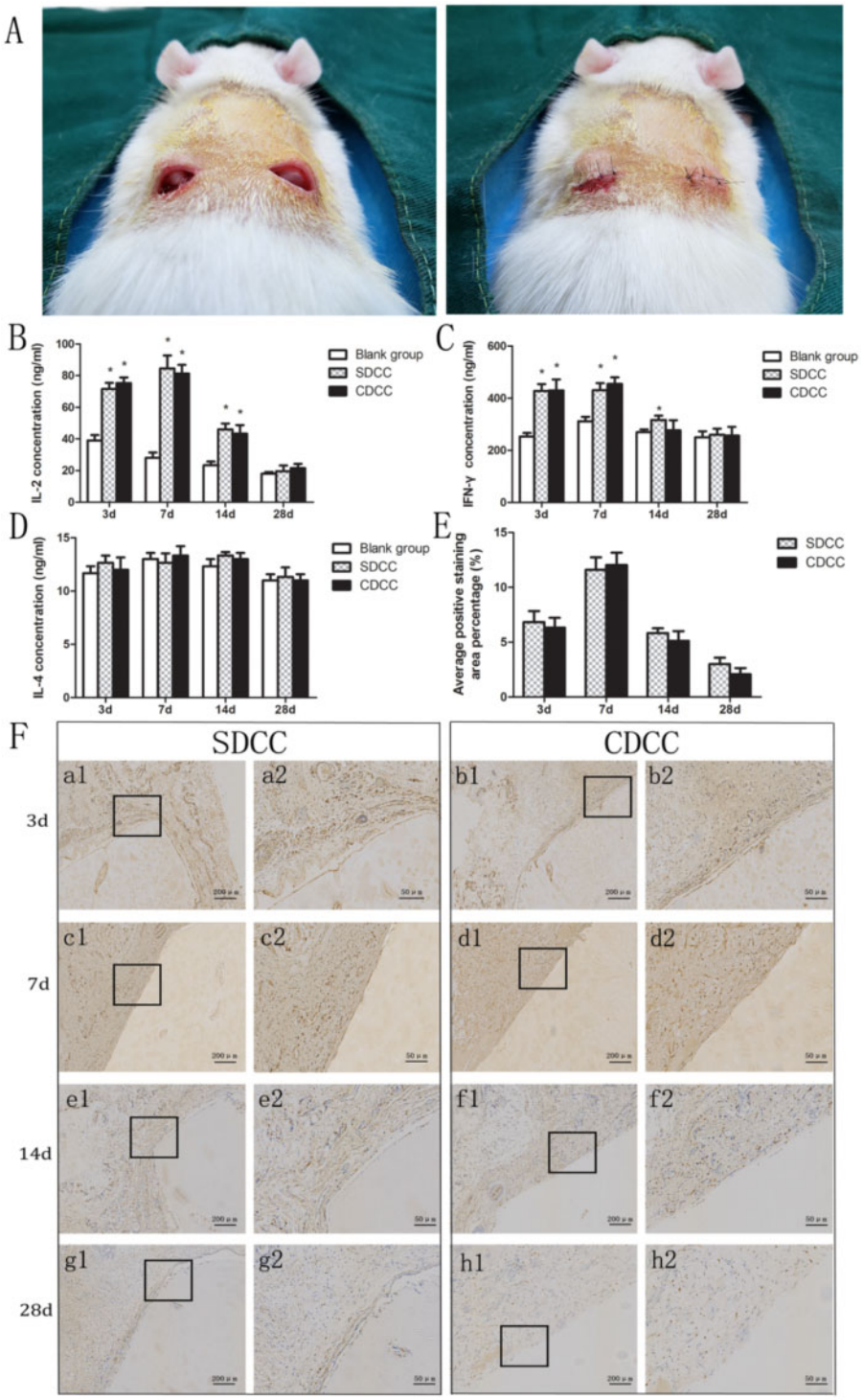


**Figure 6.** *In vivo* biocompatibility assay. (**A**) Subcutaneous implantation experiment. IL-2 (**B**), IFN-γ (**C**) and IL-4 (**D**) concentrations in serum of the Sprague-Dawley rats implanted with SDCC and CDCC. $^{*}P < 0.05$ compared with blank group. (**E**) Quantification of immunohistochemical staining by CD 11b positive cell counting at ×400. (**F**) Immunohistochemical staining of graft and adjacent tissue. It exhibited the density and distribution of CD11b (+) neutrophils in the early stage of *in vivo* implantation. Images with higher magnification (×400) (scale bar = 50μm) represent the area indicated by the black box in lower magnification images (×100) (scale bar = 200μm).

staining showed that the number of CD 11b (+) cells in SDCC and CDCC groups followed a trend of first increasing and then decreasing. At four time points, the density of positive cells in both groups was comparable ($P > 0.05$) (Fig. 6E).

## Functionality study

***Imaging assessment.*** MRI of the rabbit's nose area was performed at 3 and 6 months after surgery to investigate the graft morphology and compatibility with surrounding tissues. Comparing the MRI at 3 and

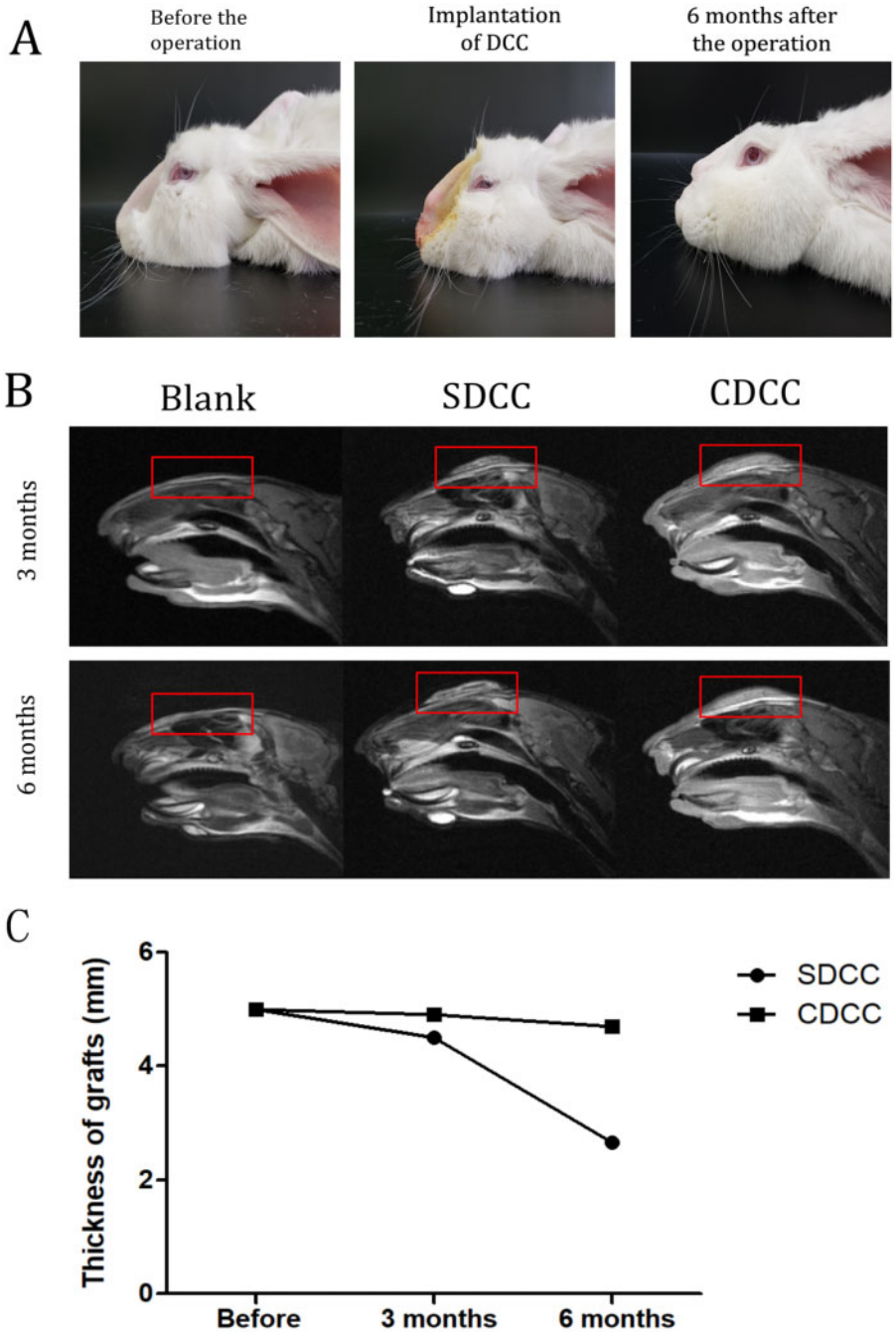


**Figure 7.** Observation of the effect of CDCC and SDCC implanted in the nasal area. (**A**) The morphological changes of the nasal dorsum of rabbits before, in and 6 months after the operation. (**B**) Comparison of MRI image between SDCC and CDCC 3 and 6 months after implantation. (**C**) The changes in the volume of SDCC and CDCC.

6 months after operation, the grafts in the SDCC group became significantly smaller, while the grafts in the CDCC group remained stable with no significant changes or slightly shrunk. At 3 months after surgery, liquefaction occurred around the graft in the SDCC group, while the graft in the CDCC group was closely connected to the surrounding tissues. At 6 months after surgery, a liquefaction zone appeared in the center of SDCC, suggesting that degradation occurred in the SDCC group (Fig. 7B). On the contrary, the graft in CDCC group maintained a uniform density without liquefaction or necrosis. Moreover, the graft of CDCC was tightly attached to the surrounding tissues, forming bio-combination, without significant degradation, indicating that the graft has good biocompatibility (Fig. 7B).

The volume changes of the grafts were evaluated using MRIs. After implantation, the thickness of SDCC decreased significantly, and by 6 months after surgery, it was 53% of the preoperative thickness. After 6 months of *in vivo* implantation, the thickness of the CDCC was slightly reduced, which was 94% of the preoperative value, with no statistical difference. The CDCC graft basically maintained its shape without significant degradation, and withstood the pressure from the skin of the nose (Fig. 7C).

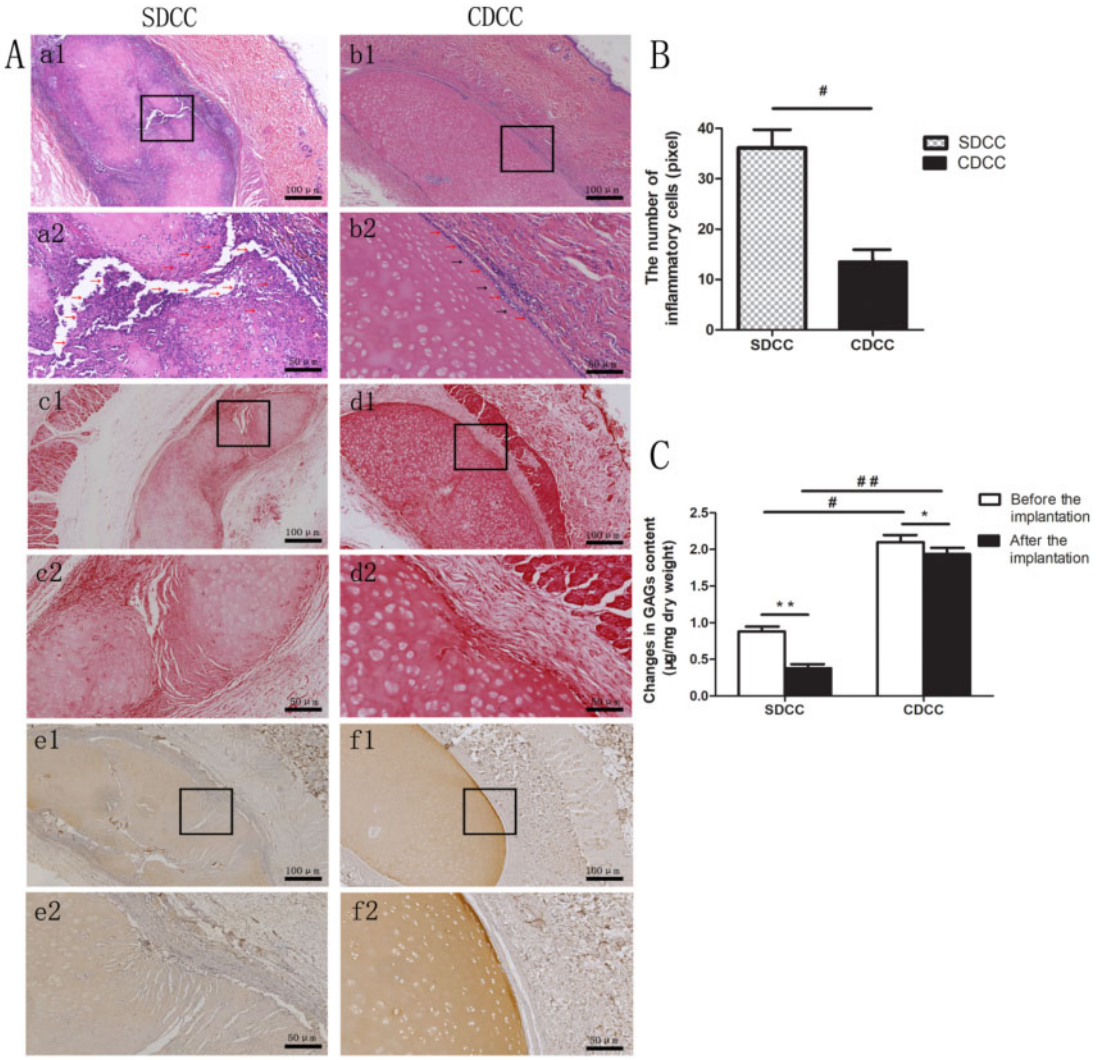


**Figure 8.** Histological staining 6 months after implantation *in vivo*. (**A**) HE, Safranin O and type II collagen immunohistochemical staining revealed the histological changes in SDCC and CDCC 6 months after nasal implantation (a–b: HE, c–d: Safranin O, e–f: type II collagen immunohistochemical staining). Images with higher magnification (×200) (scale bar = 50μm) (a2, b2, c2, d2, e2, f2) represent the area within the black box in lower magnification images (×100) (scale bar = 100μm) (a1, b1, c1, d1, e1, f1). (**B**) The number of inflammatory cells in CDCC and SDCC. #$P < 0.05$ compared with SDCC. (**C**) The content of GAGs in SDCC and CDCC. $^{*}P < 0.05$, $^{**}P < 0.01$compared with that before implantation, $^{\#}P < 0.05$, $^{\#\#}P < 0.01$ compared with SDCC.

***Assessment of degradation and inflammatory response***. The HE staining at 6 months after surgery demonstrated that the SDCC group had a large number of inflammatory cell invasion around the graft, and there were large degradation fissures in the central area, in which massive cells invaded (Fig. 8A, a1, a2). In the contrast, in the CDCC group, a small amount of inflammatory cells were present on the surface of the graft as indicated by the red arrows, without significant degradation (Fig. 8a, b1, b2). The inflammatory cell count analysis also confirmed that the number of inflammatory cells in the CDCC group was dramatically lower than that in the SDCC group (*in*) (Fig. 8B). In addition, a small number of host cells appeared in the superficial area of the grafts in the CDCC group (2–3 cells in thickness) as indicated by the black arrows (Fig. 8a, b2).

***Evaluation of degradation and reconstruction in vivo.*** The change in GAG and type II collagen content reflected the dynamic result of degradation in grafts. At 6 months after surgery, Safranin O staining showed that there were more GAGs in the CDCC group than in the SDCC group, especially in the superficial zone of CDCC, while SDCC grafts showed obvious light staining due to being degraded (Fig. 8A, c1, c2, d1, d2). Furthermore, GAGs quantitative analysis proved that the content of GAGs in the CDCC group was significantly higher than that of SDCC after 6 months of implantation, and the difference was more significant than before implantation ($P < 0.01$) (Fig. 8C). Moreover, the immunohistochemical staining of type II collagen confirmed that the collagen structure of the CDCC graft was preserved relatively intact, and a small amount of new collagen presented in the superficial area. However, there are large fissures in the collagen structure of SDCC, in which too fast degradation and absorption occurred (Fig. 8A, e1, e2, f1, f2). The above results demonstrated that after 6 months of *in vivo* implantation, ECM in the CDCC was basically retained without severe absorption, compared with SDCC.

## Discussion

To date, due to the excellent biocompatibility, autologous costal cartilage is widely used in rhinoplasty [21–23]. However, recipients increasingly refuse to accept the huge trauma caused by the cutting of costal tissue in the pursuit of nasal beauty [24–26]. Limited by the various shortcomings of autologous cartilage, researchers have been looking forward to an alternative material, which enables recipients to avoid the pain and trauma caused by costal cartilage surgery [27–29]. Decellularized tissue materials derived from xenogeneic sources have the characteristics of easy availability, low immunogenicity and high biocompatibility, and are promising alternatives to autologous tissues [30–33]. Conventional cartilage decellularization protocols include chemical and physical methods. Chemical treatment mainly refers to repeated washing with ionic detergents, which results in a large loss of effective ECM components. Although the physical method has little adverse effect on the matrix, it has been limited for its low efficiency when applied to cartilage tissue, which requires a long time and multiple cycles of freezing and thawing. To overcome the problems caused by these conventional protocols, this study tried to replace sodium deoxycholate with trypsin. Trypsin has the ability to cause chondroitin to lose its attachment activity, which plays an important role in the binding of cells and ECM [34]. This enzymatic reagent, which is commonly used to digest cells during cell passage, has low toxicity and its activity is easily terminated. The present study devised an improved decellularization protocol capitalizing on the combination of enzymatic incubation and the treatment of mild non-ionic detergents, and successfully fabricated an optimized decellularized costal cartilage. Our goal is to combine these methods to coordinate the balance between xenogeneic antigen removal and ECM component preservation for promoting the therapeutic effect and clinical application potential of decellularized cartilage [35].

Excessive remnant cellular or nuclear components are prone to elicit unfavorable immune responses, which can lead to rejection of xenogeneic grafts [36, 37]. In this study, it was proven that no residual cell and nucleus could be detected in CDCC and SDCC, and the remnant DNA contents were significantly decreased to less than 50 ng/mg, without DNA fragment greater than 200 bp. These results indicated that the optimized decellularization protocol was capable of elimination of cellular components as effective as the conventional protocol, and the optimized graft could meet the criterion of Crapo *et al*. [10].

To identify the impact of the two methods on cartilage ECM, quantitative and qualitative detections of total collagen and GAGs were performed. Concerning total collagen content, there was no statistically significant difference in three groups of NCC, SDCC and CDCC. In terms of GAGs, the contents of SDCC and CDCC were significantly lower than that of NCC. But the presence of remarkably more GAGs was detected in CDCC than SDCC, consistent with the result observed by Safranin O staining, which was mainly due to the mild processing of the modified protocol. The retention of cartilage components, especially the highly hydrophilic GAGs, is more conducive to the maintenance of physical properties of CDCC [38–41]. Furthermore, as demonstrated by previous studies, GAGs combine with collagen to wrap collagen fibers on the surface of the cartilage, acting as a molecular sieve filter and protecting the cartilage from the attack of degrading enzymes [42]. Once the GAGs are eliminated and rupture appear in the cartilage surface, the potential risk of cartilage destruction is greatly increased. Therefore, preserving more GAGs is essential to maintain the mechanical properties and protect cartilage grafts from degradation and inflammation.

On the basis of preserving ECM components, the graft prepared by the improved method retained better mechanical properties. Although the Young's modulus and stress at fracture of CDCC were lower than that of NCC, they were significantly higher than that of SDCC. Moreover, it is worth mentioning that the Young's modulus of CDCC was closer to that of human septal cartilage (9.71 MPa). The fracture stress of CDCC was also significantly higher than that of SDCC, indicating that CDCC was better than SDCC in withstanding external force deformation. Possessing proper elasticity, compression resistance and stability is one of the essential requirements for rhinoplasty prosthesis, which allows the graft to withstand the pressure from the skin and other surrounding tissues and contributes to the maintenance of the graft shape [43, 44].

Regarding biocompatibility and biosecurity, this study conducted *in vitro* tests, including cell affinity, DNA released in culture medium [45] and CCK-8 assay [46], as well as *in vivo* tests, including inflammatory factor ELISA and neutrophil immunohistochemical staining [47]. The possible reasons for immune rejection and cytotoxicity of decellularized ECM materials mainly include residual cell components and toxic substances remaining in the process of decellularization and sterilization [20, 48, 49]. The results confirmed that CDCC and SDCC had excellent cell compatibility and did not cause severe acute systemic and local immune responses.

Owing to the tissue level and area size of the nasal dorsum similar to that of the human body, rabbits were selected as the animal model of simulated rhinoplasty surgery to further study the *in vivo* functionalities of grafts [50]. MRI results showed that liquefied zone appeared at 3 months after implantation in SDCC, and absorption and degradation became obvious after 6 months, while CDCC roughly maintained its original morphology during 6 months of implantation with no significant degradation or slight contraction. HE staining revealed that there were a large number of inflammatory cells in the marginal zone of SDCC after 6 months of implantation, which was mainly due to the degradation products produced by the excessive degradation of the graft [51, 52]. In addition, inflammatory cell invasion also appeared in the center of the graft, which destroyed the original structure and caused liquefaction in the central zone.

The histological staining of Safranine O and type II collagen demonstrated that the content and distribution of the main components of ECM in CDCC have less changes compared with ruptured SDCC, with no obvious absorption and degradation. Besides, the comparison of preoperative and postoperative GAGs content exhibited that the GAGs content of SDCC and CDCC groups both decreased after the implantation. However, the reduction was more obvious in the SDCC group, which further confirmed that SDCC had significant degradation and absorption, while the GAGs in the CDCC group maintained 90.47% of the pre-implantation content. In SDCC group, the lack of bioactive ECM components and insufficient mechanical strength led to excessive degradation of the graft, which in turn resulted in chronic inflammation. Then, the inflammatory cells turned to accelerate the rate of degradation and absorption [53, 54].

The above positive results demonstrate that the optimized decellularized grafts have great potential for clinical application. As a preliminary attempt of the optimization and application of xenogeneic costal cartilage, there is still a lot of work waiting to be perfected [55]. In the future, porosity and pore size need to be further improved by puncture or laser to provide favorable conditions for the host cell migration or exogenous cell co-culture. Besides, the prospect of xenogeneic acellular costal cartilage applied to other cartilage defects such as microtia remains to be studied and explored.

## Conclusion

The present study suggested that the optimized decellularized costal cartilage fabricated by the modified protocol preserved more structural components, with effective removal of cellular components. Meanwhile, the mechanical properties of CDCC were more stable, which was more conducive to maintaining the morphology and bearing the load. The *in vitro* and *in vivo* biosecurity studies showed that the optimized CDCC had excellent biocompatibility, and was confirmed to possess a better capacity to slow down the degradation rate, reduce the inflammation response and maintain the graft morphology in comparison with SDCC. In summary, the feasibility of acellular cartilage as a rhinoplasty graft was comprehensively evaluated for the first time, and few similar studies have been reported before. This work provides an innovative perspective for the future in-depth investigation of decellularized costal cartilage, and contributes to the advancement of alternative strategies for rhinoplasty prosthesis.

## Acknowledgments

This work was supported by Sichuan Science and Technology Program (2020YFH0008); National Natural Science Foundation of China (No. 81771351); Joint Research Fund Liaoning-Shenyang National Laboratory for Materials Science (2019JH3/3010 0 022) and National Key R&D Program of China (2017YFA0105802).

*Conflict of interest statement*. None declared.

## References

1. Bellinga RJ, Capitan L, Simon D *et al.* Technical and clinical considerations for facial feminization surgery with rhinoplasty and related procedures. *JAMA Facial Plast Surg* 2017;**19**:175–81.
2. Bender-Heine AN, Zdilla MJ, Russell ML *et al.* Optimal costal cartilage graft selection according to cartilage shape: anatomical considerations for rhinoplasty. *Facial Plast Surg* 2017;**33**:670–4.
3. Wee JH, Mun SJ, Na WS *et al.* Autologous vs irradiated homologous costal cartilage as graft material in rhinoplasty. *JAMA Facial Plast Surg* 2017;**19**:183–8.
4. Bhat U, Garg S, D'Souza EJ *et al.* Precision carving of costal cartilage graft for contour fill in aesthetic and reconstructive rhinoplasty. *Indian J Plast Surg* 2014;**47**:25–35.
5. Ozucer B, Dinc ME, Paltura C *et al.* Association of autologous costal cartilage harvesting technique with donor-site pain in patients undergoing rhinoplasty. *JAMA Facial Plast Surg* 2018;**20**:136–40.
6. Kim BS, Das S, Jang J *et al.* Decellularized extracellular matrix-based bioinks for engineering tissue- and organ-specific microenvironments. *Chem Rev* 2020;**120**:10608–61.
7. Gawlitta D, Benders KE, Visser J *et al.* Decellularized cartilage-derived matrix as substrate for endochondral bone regeneration. *Tissue Eng Part A* 2015;**21**:694–703.
8. Sun Y, Yan L, Chen S *et al.* Functionality of decellularized matrix in cartilage regeneration: a comparison of tissue versus cell sources. *Acta Biomater* 2018;**74**:56–73.
9. Rowland CR, Colucci LA, Guilak F. Fabrication of anatomically-shaped cartilage constructs using decellularized cartilage-derived matrix scaffolds. *Biomaterials* 2016;**91**:57–72.
10. Crapo PM, Gilbert TW, Badylak SF. An overview of tissue and whole organ decellularization processes. *Biomaterials* 2011;**32**:3233–43.
11. Gilbert TW, Sellaro TL, Badylak SF. Decellularization of tissues and organs. *Biomaterials* 2006;**27**:3675–83.
12. Shen W, Berning K, Tang SW *et al.* Rapid and detergent-free decellularization of cartilage. *Tissue Eng Part C Methods* 2020;**26**:201–6.
13. Guruswamy Damodaran R, Vermette P. Tissue and organ decellularization in regenerative medicine. *Biotechnol Prog* 2018;**34**:1494–505.
14. Hillebrandt KH, Everwien H, Haep N *et al.* Strategies based on organ decellularization and recellularization. *Transpl Int* 2019;**32**:571–85.
15. Giraldo-Gomez DM, Leon-Mancilla B, Del Prado-Audelo ML *et al.* Trypsin as enhancement in cyclical tracheal decellularization: morphological and biophysical characterization. *Mater Sci Eng C Mater Biol Appl* 2016;**59**:930–7.
16. Phelan MC. Techniques for mammalian cell tissue culture. *Curr Protoc Hum Genet* 2007;**33**:A.3B.1-A.3B.18.
17. de Aluja AS. [Laboratory animals and official Mexican norms (NOM-062-ZOO-1999)]. *Gac Med Mex* 2002;**138**:295–8.
18. Baiguera S, Jungebluth P, Burns A *et al.* Tissue engineered human tracheas for in vivo implantation. *Biomaterials* 2010;**31**:8931–8.
19. Dettin M, Zamuner A, Naso F *et al.* Natural scaffolds for regenerative medicine: direct determination of detergents entrapped in decellularized heart valves. *Biomed Res Int* 2017;**2017**:9274135.
20. Cebotari S, Tudorache I, Jaekel T *et al.* Detergent decellularization of heart valves for tissue engineering: toxicological effects of residual detergents on human endothelial cells. *Artif Organs* 2010;**34**:206–10.
21. Park JH, Jin HR. Use of autologous costal cartilage in Asian rhinoplasty. *Plast Reconstr Surg* 2012;**130**:1338–48.
22. Horton CE, Matthews MS. Nasal reconstruction with autologous rib cartilage: a 43-year follow-up. *Plast Reconstr Surg* 1992;**89**:131–5.
23. Zhang L, Ma WS, Bai JP *et al.* Comprehensive application of autologous costal cartilage grafts in rhino- and mentoplasty. *J Craniofac Surg* 2019;**30**:2174–7.
24. Ho TT, Sykes K, Kriet JD *et al.* Cartilage graft donor site morbidity following rhinoplasty and nasal reconstruction. *Craniomaxillofac Trauma Reconstr* 2018;**11**:278–84.
25. Moon BJ, Lee HJ, Jang YJ. Outcomes following rhinoplasty using autologous costal cartilage. *Arch Facial Plast Surg* 2012;**14**:175–80.
26. Varadharajan K, Sethukumar P, Anwar M *et al.* Complications associated with the use of autologous costal cartilage in rhinoplasty: a systematic review. *Aesthet Surg J* 2015;**35**:644–52.
27. Vila PM, Jeanpierre LM, Rizzi CJ *et al.* Comparison of autologous vs homologous costal cartilage grafts in dorsal augmentation rhinoplasty: a systematic review and meta-analysis. *JAMA Otolaryngol Head Neck Surg* 2020;**146**:347–54.
28. Kim YK, Kania K, Nguyen AH. Rhinoplasty with cartilage and alloplastic materials, nasal SMAS management in Asian rhinoplasty, contracture classification, and secondary rhinoplasty with contracture. *Semin Plast Surg* 2015;**29**:255–61.
29. Liang X, Wang K, Malay S *et al.* A systematic review and meta-analysis of comparison between autologous costal cartilage and alloplastic materials in rhinoplasty. *J Plast Reconstr Aesthet Surg* 2018;**71**:1164–73.
30. Luc G, Charles G, Gronnier C *et al.* Decellularized and matured esophageal scaffold for circumferential esophagus replacement: proof of concept in a pig model. *Biomaterials* 2018;**175**:1–18.
31. Porzionato A, Stocco E, Barbon S *et al.* Tissue-engineered grafts from human decellularized extracellular matrices: a systematic review and future perspectives. *Int J Mol Sci* 2018;**19**: 4117.
32. Davila AA, Seth AK, Wang E *et al.* Human acellular dermis versus submuscular tissue expander breast reconstruction: a multivariate analysis of short-term complications. *Arch Plast Surg* 2013;**40**:19–27.
33. Valdatta L, Cattaneo AG, Pellegatta I *et al.* Acellular dermal matrices and radiotherapy in breast reconstruction: a systematic review and meta-analysis of the literature. *Plast Surg Int* 2014;**2014**:472604.
34. Rahman S, Griffin M, Naik A *et al.* Optimising the decellularization of human elastic cartilage with trypsin for future use in ear reconstruction. *Sci Rep* 2018;**8**:3097.
35. Gilbert TW. Strategies for tissue and organ decellularization. *J Cell Biochem* 2012;**113**:2217–22.
36. Badylak SF. Decellularized allogeneic and xenogeneic tissue as a bioscaffold for regenerative medicine: factors that influence the host response. *Ann Biomed Eng* 2014;**42**:1517–27.

37. Keane TJ, Londono R, Turner NJ *et al.* Consequences of ineffective decellularization of biologic scaffolds on the host response. *Biomaterials* 2012; **33**:1771–81.
38. Cheng CW, Solorio LD, Alsberg E. Decellularized tissue and cell-derived extracellular matrices as scaffolds for orthopaedic tissue engineering. *Biotechnol Adv* 2014;**32**:462–84.
39. Sutherland AJ, Converse GL, Hopkins RA *et al.* The bioactivity of cartilage extracellular matrix in articular cartilage regeneration. *Adv Healthc Mater* 2015;**4**:29–39.
40. Patel JM, Saleh KS, Burdick JA *et al.* Bioactive factors for cartilage repair and regeneration: improving delivery, retention, and activity. *Acta Biomater* 2019;**93**:222–38.
41. Gillies AR, Lieber RL. Structure and function of the skeletal muscle extracellular matrix. *Muscle Nerve* 2011;**44**:318–31.
42. Figueres Juher T, Bases Perez E. [An overview of the beneficial effects of hydrolysed collagen intake on joint and bone health and on skin ageing]. *Nutr Hosp* 2015;**32 Suppl 1**:62–6.
43. Zeng Y, Wu W, Yu H *et al.* Silicone implant in augmentation rhinoplasty. *Ann Plast Surg* 2002;**49**:495–9.
44. Yang J, Wang X, Zeng Y *et al.* Biomechanics in augmentation rhinoplasty. *J Med Eng Technol* 2005;**29**:14–7.
45. Locci P, Marinucci L, Lilli C *et al.* Biocompatibility of alloys used in orthodontics evaluated by cell culture tests. *J Biomed Mater Res* 2000;**51**: 561–8.
46. Qian Y, Zhou X, Zhang F *et al.* Triple PLGA/PCL scaffold modification including silver impregnation, collagen coating, and electrospinning significantly improve biocompatibility, antimicrobial, and osteogenic properties for orofacial tissue regeneration. *ACS Appl Mater Interfaces* 2019;**11**:37381–96.
47. He J, Li Z, Yu T *et al.* In vitro and in vivo biocompatibility study on acellular sheep periosteum for guided bone regeneration. *Biomed Mater* 2020; **15**:015013.
48. Hussein KH, Park KM, Kang KS *et al.* Biocompatibility evaluation of tissue-engineered decellularized scaffolds for biomedical application. *Mater Sci Eng C Mater Biol Appl* 2016;**67**:766–78.
49. Kraft L, Ribeiro VST, de Nazareno Wollmann LCF *et al.* Determination of antibiotics and detergent residues in decellularized tissue-engineered heart valves using LC-MS/MS. *Cell Tissue Bank* 2020;**21**:573–84.
50. Moon KC, Han SK. Surgical anatomy of the Asian nose. *Facial Plast Surg Clin North Am* 2018;**26**:259–68.
51. Badylak SF, Gilbert TW. Immune response to biologic scaffold materials. *Semin Immunol* 2008;**20**:109–16.
52. Morris AH, Stamer DK, Kyriakides TR. The host response to naturally-derived extracellular matrix biomaterials. *Semin Immunol* 2017;**29**:72–91.
53. Keane TJ, Badylak SF. The host response to allogeneic and xenogeneic biological scaffold materials. *J Tissue Eng Regen Med* 2015;**9**:504–11.
54. Chung L, Maestas DR Jr, Housseau F *et al.* Key players in the immune response to biomaterial scaffolds for regenerative medicine. *Adv Drug Deliv Rev* 2017;**114**:184–92.
55. Nouri Barkestani M, Naserian S, Uzan G *et al.* Post-decellularization techniques ameliorate cartilage decellularization process for tissue engineering applications. *J Tissue Eng* 2021;**12**:2041731420983562.